

A Journal of the Gesellschaft Deutscher Chemiker

Angewandte Chemie

GDCh

International Edition

www.angewandte.org

Accepted Article

Title: Reversible CO₂ Hydrogenation, Neutron Crystallography, and Hydride Reactivity of a Triiridium Heptahydride Complex

Authors: Valeriy Cherepakhin, Van K. Do, Anthony J. Chavez, Jacob Kelber, Ryan A. Klein, Eric Novak, Yongqiang Cheng, Xiaoping Wang, Craig M. Brown, and Travis J. Williams

This manuscript has been accepted after peer review and appears as an Accepted Article online prior to editing, proofing, and formal publication of the final Version of Record (VoR). The VoR will be published online in Early View as soon as possible and may be different to this Accepted Article as a result of editing. Readers should obtain the VoR from the journal website shown below when it is published to ensure accuracy of information. The authors are responsible for the content of this Accepted Article.

To be cited as: *Angew. Chem. Int. Ed.* **2025**, e202501943

Link to VoR: <https://doi.org/10.1002/anie.202501943>

RESEARCH ARTICLE

Reversible CO₂ Hydrogenation, Neutron Crystallography, and Hydride Reactivity of a Triiridium Heptahydride ComplexValeriy Cherepakhin,^{+[a]} Van K. Do,^{+[a]} Anthony J. Chavez,^[a] Jacob Kelber,^[a] Ryan A. Klein,^[b,c] Eric Novak,^[d] Yongqiang Cheng,^[d] Xiaoping Wang,^[d] Craig M. Brown,^[c,e] and Travis J. Williams^{*[a]}

[a] Dr. V. Cherepakhin, Dr. V. K. Do, A. J. Chavez, J. Kelber, Prof. T. J. Williams
Loker Hydrocarbon Research Institute, Wrigley Institute for Environment and Sustainability, and Department of Chemistry
University of Southern California
Los Angeles, California 90089-1661, USA
E-mail: travisw@usc.edu

[b] Dr. R. A. Klein
Material, Chemical, and Computational Sciences Directorate
National Renewable Energy Laboratory
Golden, Colorado 80401, USA

[c] Dr. R. A. Klein, Dr. C. M. Brown
Center for Neutron Research
National Institute of Standards and Technology
Gaithersburg, Maryland 20899, USA

[d] Dr. E. Novak, Dr. Y. Cheng, Dr. X. Wang
Spallation Neutron Source, Neutron Scattering Division
Oak Ridge National Laboratory
Oak Ridge, Tennessee 37831, USA

[e] Prof. C. M. Brown
Department of Chemical and Biomolecular Engineering
University of Delaware
Newark, Delaware 19716, USA

[+] These authors contributed equally to this work.

Supporting information for this article is given via a link at the end of the document.

Abstract: We report the structure, reactivity, and catalytic utility of a triiridium complex, $[\text{Ir}_3\text{H}_6(\mu_3\text{-H})(\text{PN})_3]^{2+}$ (**2-H**, $\text{PN} = (2\text{-pyridyl})\text{CH}_2\text{P}(\text{Bu})_2$). Despite its unusual stability to unsaturated organics, electrophiles, and even $\text{CF}_3\text{SO}_3\text{D}$, we find that complex **2-H** catalyzes hydrogenation of CO_2 to formate ($\text{TON}_{\text{Ir}} = 9,600$) and reverse formic acid dehydrogenation ($\text{TON}_{\text{Ir}} = 54,400$). The hydrogenation operates via a reactive intermediate $[\text{Ir}_3\text{H}_4(\mu\text{-H})_4(\text{PN})_3]^+$ (**5**). Neutron crystallography and DFT-supported neutron vibrational spectroscopy of **2-H** reveal Ir–H bond lengths and elucidate the vibration modes within the Ir_3H_7 core. Stoichiometric oxidation of **2-H** produces four classes of iridium complexes of varied nuclearity and hydride structure; tetra- and pentanuclear clusters $[\text{Ir}_3\text{H}_6(\mu_3\text{-AuPPh}_3)(\text{PN})_3]^{2+}$ (**2-Au**) and $[\text{Ag}(\text{Ir}_2\text{H}_4(\mu\text{-OAc})(\text{PN})_2)_2]^{3+}$ (**6**) were generated using AuPPh_3^+ and AgOAc , respectively. Further oxidation to class $[\text{Ir}_2\text{H}_3(\mu\text{-X})_2(\text{PN})_2]^+$ is possible with AgOAc , $\text{Hg}(\text{OAc})_2$, or I_2 . Finally, a TEMPO/HCl system completely oxidizes the hydrides and gives $[\text{Ir}_2\text{Cl}_4(\mu\text{-Cl})_2(\text{PN})_2]$ (**11**).

longevity in CO_2 hydrogenation ($\text{TOF} < 2 \times 10^5 \text{ h}^{-1}$, $\text{TON} < 4 \times 10^6$)^[6] and formic acid dehydrogenation ($\text{TOF} < 5 \times 10^5 \text{ h}^{-1}$, $\text{TON} < 3 \times 10^6$).^[11]

While many mono- and dinuclear iridium hydride species are known, there are only a few reports on triiridium heptahydrides $[\text{Ir}_3\text{H}_6(\mu_3\text{-H})\text{L}_6]^{2+}$.^[12–16] These feature a high thermal stability and their trinuclear scaffold is retained upon treatment with strong π -accepting ligands (e.g., CO , C_2H_4 , CD_3CN , and *p*- ToINC).^[13–15] Moreover, the inability of the complexes to dissociate to monomers was inferred from their catalytic inertness in the alkene hydrogenation.^[12,16] Yet, we hypothesized that the Ir_3H_7 clusters might have interesting catalytic properties enabled by the metal-metal cooperation under the right conditions. In this study, we demonstrate a catalytic activity of a new triiridium heptahydride complex **2-H** (Figure 1) in reversible hydrogenation of CO_2 to formate. The complex is derived from precursor **1**, which has been extensively studied in our group.^[16–20] We also report a stoichiometric reactivity study on **2-H** that illustrates the stability and dissociation of the trinuclear scaffold under oxidative conditions.

Introduction

Hydrogenation of CO_2 to formic acid and the reverse reaction catalyzed by transition metal complexes have been extensively studied due to the potential use of formic acid as a liquid organic hydrogen carrier.^[1,2] The reported Ir-based catalysts are derivatives of Cp^*Ir ,^[3] $(\text{COD})\text{Ir}$,^[4,5] and octahedral $\text{Ir}(\text{III})$ ^[6] bearing bi-, tri-, and tetradentate^[7] ligands with donors such as *N*-heterocycles, NHCs,^[8] and phosphines.^[5,6] Many of these ligands are pH-responsive and thus, enable the metal-ligand cooperative catalysis.^[9,10] Some of the iridium catalysts show high activity and

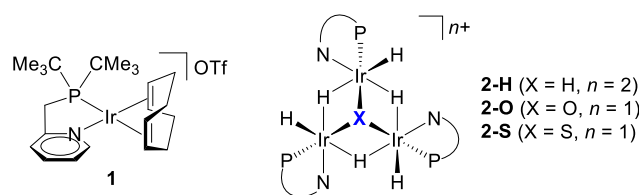


Figure 1. Complexes studied in this work.

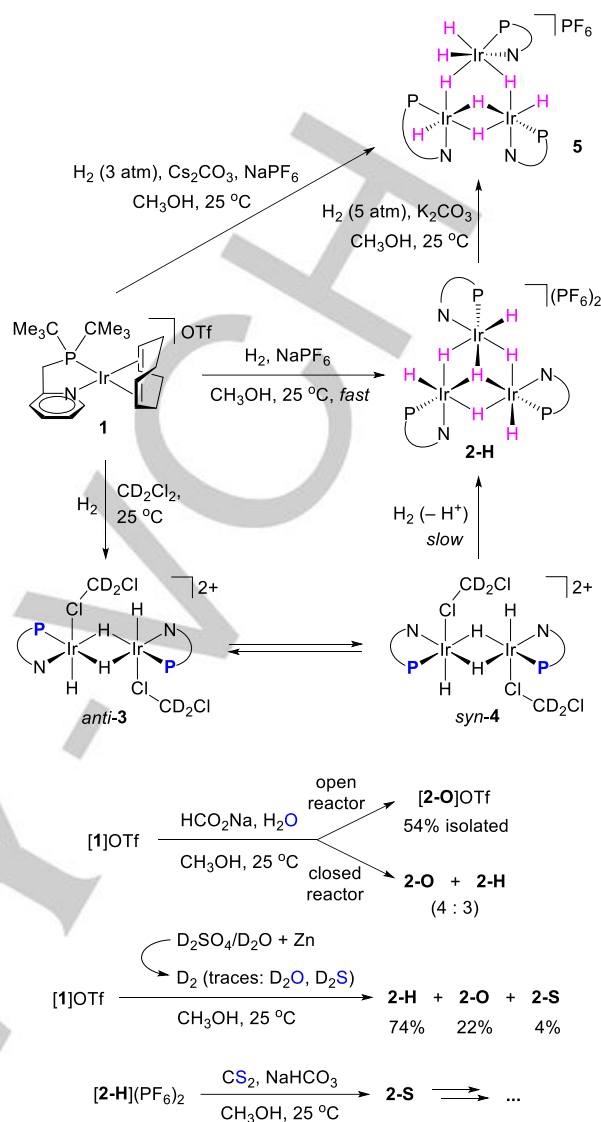
RESEARCH ARTICLE

Results and Discussion

Formation of Trinuclear Iridium Hydrides. We prepared compounds **[2-H](PF₆)₂**, **[2-H](OTf)₂**, **[2-H-d₇](PF₆)₂**, and **[2-H-d₇](PF₆)₂** in 80–90% yields by hydrogenating the corresponding Ir(I) precursors **[1]OTf** or **[1-d₂₄]OTf** under ambient conditions (Scheme 1).^[12–16] While complex **2-H** forms quickly in methanol (ca. 10 min), the reaction slows in an aprotic CH₂Cl₂ environment affording evidence of isomeric dinuclear intermediates *anti*-**3** and *syn*-**4** with the composition [Ir₂H₂(μ-H)₂(CD₂Cl₂)₂(PN)₂]²⁺ (Table S3).^[21,22] A time course ¹H NMR study (Figure S62) shows rapid conversion of **1** to *anti*-**3**, with concurrent full hydrogenation of cyclooctadiene, within 1 hour. A dynamic equilibrium between *anti*-**3** and *syn*-**4** (1:1) is then established within 10 hours, which does not change as the reaction continues. Finally, a slow, zero-order conversion of the isomers gives **2-H** in 25% NMR yield after 56 hours.

We found that [Ir₃H₃(μ-H)₃(μ₃-H)(PN)₃]²⁺ (**2-H**) readily adds an extra hydride ligand to form [Ir₃H₄(μ-H)₄(PN)₃]⁺ (**5**), which seems to be the ultimately hydrogenated form of the Ir₃ cluster (Scheme 1). When **1** or **2-H** are pressurized (1–10 atm) with H₂ in a methanolic carbonate solution, poorly soluble **[5]PF₆** is crystallized, which can be isolated in 53% yield. The crystal structure of **5** suggests the addition of one terminal hydride accompanied by dissociation of Ir–(μ₃-H) bond and rearrangement of the three PN ligands during the **2-H** to **5** conversion (Figure S70). ¹H NMR spectrum of **5** shows well-resolved signals of eight unique hydrides (Figure S25), indicating retention of the asymmetric cluster structure in CD₂Cl₂ solution. The dissociation of Ir–(μ₃-H) bond within Ir₃H₇ cluster was also observed during carbonylation of analogous [Ir₃H₇(dppp)₃]²⁺ to [Ir₃H₇(CO)(dppp)₃]²⁺.^[15]

Derivatives of complex **2-H**, in which μ₃-H is replaced by a heteroatom, [Ir₃H₃(μ-H)₃(μ₃-E)(PN)₃]⁺ (E = O and S), can be easily accessed from **1** or **2-H** (Scheme 1). We first encountered an oxo-centered triiridium cluster [Ir₃H₆(μ₃-O)(PN)₃]⁺ (**2-O**) in experiments on methanol dehydrogenation using **[1]OTf** as a catalyst. Thus, compound **[2-O]OTf** is obtained in 54% yield by reacting **[1]OTf** with sodium formate in aqueous methanol. Complex **2-O** features three equivalent Ir^{III}(PN) fragments bound by a triply-bridging pyramidal oxygen atom characterized by Ir–O distance of 2.0713(18) Å and Ir–O–Ir angle of 86.32(9)° (X-ray, Figure S70). ¹H NMR shows two signals at –22.03 (3H) and –22.49 ppm (3H), corresponding to bridging and terminal hydrides. While there are several complexes with Ir₃(μ₃-O) core, **2-O** is the first example of clusters [Ir₃H₆(μ₃-O)L₆]⁺. We observe clean conversion of **1** to **2-O** only when the reactor is open to N₂ atmosphere, whereas in a closed system the reaction gives **2-O** and **2-H** in 4:3 ratio. Generally, preparation of complexes [Ir₃H₇L₆]²⁺ from Ir(I) precursors requires H₂ gas;^[12–16] therefore, **2-H** could form due to formate dehydrogenation that accumulates H₂ in the closed system. In our hands, **2-O** is not readily formed from **2-H**, despite being its apparent oxidized form.



Scheme 1. Hydrogenation of **[1]OTf**. Complexes **2-H**, **2-O**, and **5** were characterized by X-ray crystallography (Figure S70).

Isotopic labeling experiments (Table 1) establish the synthetic origin of each hydride in **2-O**. Deuteration of the CH₃ group in methanol has no effect on the yield or deuteration of **2-O** (entries 3 and 4): methanol dehydrogenation is not a step in its formation. Conversely, formate dehydrogenation is kinetically relevant, as manifested by a strong kinetic isotope effect at its CH site (entries 1 and 3). However, deuterium incorporated in **2-O** does not originate from DCOO[−] (entry 2); it derives from H⁺/D⁺ exchange with O-deuterated solvent, as exemplified in entries 3 and 4. This unusual observation supports a view that H/D exchange mechanistically precedes cluster formation because we see equal deuteration of terminal and bridging hydrides in **2-O**. Surprisingly, the deuterium content in the Ir₃H₆ fragment does not exceed 39%, even when no extra ¹H is added to the system (entry 1). We explain this by the participation of cyclooctadiene-*h*₁₂ and CH₂ groups of PN ligands in H/D exchange.

RESEARCH ARTICLE

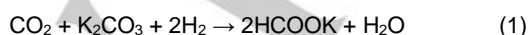
Table 1. Isotopic labeling of complex **2-O**^[a]

Entry	Reagents	NMR yield of 2-O (%) ^[b]	Deuteration of Ir ₃ H ₆ (%) ^[c]
1	D ₂ CO ₂ Na, CD ₃ OD, D ₂ O	4	39
2	D ₂ CO ₂ Na, CH ₃ OH, H ₂ O	28	0
3	HCO ₂ Na, CD ₃ OD, D ₂ O	51	30
4	HCO ₂ Na, CH ₃ OH, D ₂ O	47	39
5	HCO ₂ Na, CD ₃ OH, H ₂ O	64	0

[a] Conditions: [1]OTf (20 mg), Na-formate (20 mg), methanol (0.3 mL), and water (0.3 mL) were stirred under N₂ for 3 h at 25 °C. Solvent removal was followed by CD₂Cl₂ (0.7 mL) addition and ¹H NMR analysis. [b] Yield% = 4 × [int. 9.9 ppm]/[int. total ArH] × 100%. [c] D% = ([int. 9.9 ppm] – [int. –22.0 ppm])/[int. 9.9 ppm] × 100%.

Sulfur-containing derivative [Ir₃H₆(μ₃-S)(PN)₃]⁺ (**2-S**) was characterized in CD₂Cl₂ solution by NMR (¹H, ³¹P) and MALDI. It was observed as a major intermediate in a reaction among **2-H**, CS₂, and NaHCO₃ in methanol (Scheme 1). Complex **2-S** is more reactive than **2-O**, as it undergoes further transformations with an excess sulfide source. Importantly, HCOO⁻ was not detected in the products: instead, multiple singlets at δ_H = 2.5–4.5 ppm may indicate the presence of oligothianes (CH₂S)_n or SCH₃ groups. Complex **2-S** forms as a minor product when [1]OTf is treated with mixtures of H₂/H₂S, HCO₂Na/H₂S, or D₂/D₂O/D₂S. The latter combination generates only the three products: **2-H** (74%), **2-O** (22%), and **2-S** (4%). These show no sign of Ir₃H₆ deuteration, again demonstrating H/D scrambling between D₂ and methanol's OH.

Catalytic Hydrogenation of CO₂. Complex **2-H** does not hydrogenate organic substrates such as 1-hexene (acetone-*d*₆, 60 °C) or acetophenone (neat, 90 °C), which is consistent with the previously reported inactivity of [Ir₃H₇L₆]²⁺ clusters.^[12,16] Nevertheless, we find that **2-H** is catalytically active in CO₂ hydrogenation and formic acid dehydrogenation (Eq. 1, 2). We tested the catalytic activity of [1]OTf, [2-O]OTf, and [2-H](PF₆)₂ in hydrogenating aqueous solutions of K₂CO₃ under 35–90 bar of H₂/CO₂ at 50–120 °C (Table 2). Complex **2-O** is the least active (TON = 141) among the three catalysts at 50 °C, while **1** and **2-H** show the same activity (entries 1–3). There is no pressure effect on the performance of **2-H** (entries 3 and 4); however, raising the temperature from 50 to 120 °C improves its TON from 459 to 7,190 (entries 4–6). To evaluate the maximum TON of **2-H**, we ran the reaction for 24, 48, and 70 hours at 120 °C (entries 6–8) and extrapolate the ultimate deactivation of **2-H** after about four days at 120 °C with a maximum TON of ca. 10k cycles per iridium atom or 30k cycles of the cluster (entry 8).

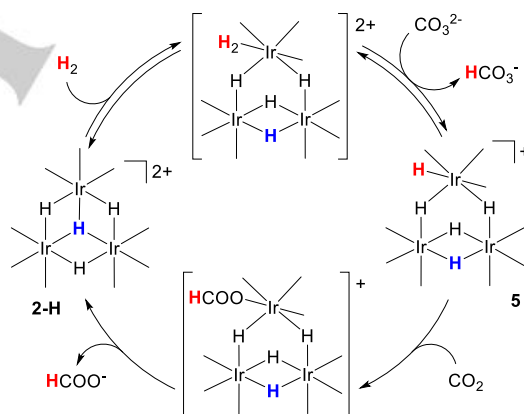


Like metal-ligand cooperation, metal-metal cooperation can also enable CO₂ hydrogenation since activation of H₂ and stabilization of the HCOO⁻ product could potentially involve coordination to multiple metal centers in a catalytic complex. Bicarbonate is not basic enough to activate the PN ligand in **2-H** by CH₂ deprotonation, so the metal-metal cooperation seems a more plausible option to access a cooperative bond activation mechanism. One such mechanism is illustrated in Scheme 2.

Table 2. Catalytic hydrogenation of CO₂ to HCOOK^[a]

Entry	Catalyst (ppm) ^[b]	P (bar) (H ₂ :CO ₂)	K ₂ CO ₃ (g)	Temp. (°C) Time (h)	Yield (%) ^[c] TON ^[d]
1	[1]OTf (101)	35 (6:1)	1.00	50 24	4 398
2	[2-O]OTf (142)	45 (7:2)	1.00	50 24	2 141
3	[2-H](PF ₆) ₂ (131)	45 (7:2)	1.00	50 24	5 382
4	[2-H](PF ₆) ₂ (131)	90 (7:2)	1.00	50 24	6 459
5	[2-H](PF ₆) ₂ (1,307)	45 (7:2)	0.10	70 24	100 765
6	[2-H](PF ₆) ₂ (131)	90 (7:2)	1.00	120 24	94 7,190
7	[2-H](PF ₆) ₂ (26)	88 (7:2)	5.00	120 48	22 8,414
8	[2-H](PF ₆) ₂ (26)	88 (1:1)	5.00	120 70	25 9,561

[a] Conditions: catalyst (1.0 mg in 1.0 mL THF), K₂CO₃, H₂O (5 mL), H₂/CO₂. [b] ppm(Ir) = [mol Ir at.]/[mol K⁺] × 10⁶. [c] Yields were derived from ¹H NMR spectra using DMF as an internal standard. Yield% = 6 × [int. HCO₂]/[int. HCONMe₂] × [mol DMF]/[mol K⁺] × 100%. [d] TON = [mol HCO₂]/[mol Ir at.]. All TONs are with respect to one Ir atom.

**Scheme 2.** Proposed mechanism of CO₂ hydrogenation catalyzed by **2-H**

We interrogated the hypothesis of Scheme 2 with ¹H NMR experiments. We find that complex **2-H** does not react with CO₂ under conditions relevant to the catalysis. Instead, it is activated via hydrogenation to **5**. The reaction between **2-H** and H₂ in methanol is reversible: complex **5** is favored (> 99%) in the presence of carbonate and H₂ pressure, while **2-H** dominates (> 99%) under CO₂ pressure (Table S1). Formate is not detected in the latter reaction because CO₂ serves as a Brønsted acid at 25 °C, rather than a hydride acceptor. When **2-H** is hydrogenated in CD₃OD, we observe H/D scrambling, in particular, generation of free HD, which necessitates a dihydrogen adduct [Ir₃H₇(HD)(PN)₃]²⁺ as an intermediate between **2-H** and **5**. The rate-limiting step of the cycle is a CO₂ insertion to **5** giving a formate derivative [Ir₃H₇(HCO₂)(PN)₃]⁺, which then expels HCOO⁻

RESEARCH ARTICLE

and regenerates the catalyst—free formate and **2-H** were detected in the solution after pressurizing **5** with CO₂ at 100 °C (Table S2). Overall, the mechanism of catalytic CO₂ hydrogenation can be described as a sequence of the fast, reversible hydride addition to **2-H**, generating the catalyst resting state **5**, followed by the slow CO₂ insertion at elevated temperature and the formate release.

Dehydrogenation of neat formic acid was performed using [**2-H**](PF₆)₂ and HCOONa co-catalyst at reflux (oil bath, 110 °C). Once fully dehydrogenated, a solid catalytic mixture was recharged with another portion of formic acid. Thus, we converted 33 mL of formic acid in 11 cycles over the course of 4 days, which corresponds to at least 54,400 turnovers per Ir atom (>163k TON per cluster). NMR studies reveal clean conversion of complex **2-H** to its post-catalytic forms in the formic acid dehydrogenation.

Inspired by the discovery of this unique reactivity, which is entirely unprecedented among analogous triiridium clusters, we set about examining **2-H** through a system of stoichiometric, crystallographic, and spectroscopic studies.

Neutron Crystallography of 2-H. We report the first single crystal neutron diffraction study on a triiridium heptahydride complex using [**2-H**](OTf)₂×CH₂Cl₂. The molecular structure of **2-H** is shown in Figure 2, and its selected interatomic distances are given in Table 3. Complex **2-H** features three Ir(III) atoms arranged around a C₃ axis. The iridium atoms adopt a distorted octahedral geometry with the bond angles ranging from 80° to 105°. The composition of **2-H** suggests the absence of Ir–Ir bonds; however, the average distance between Ir atoms (2.724(9) Å) is very close to the length of the covalent Ir–Ir bond found in Ir₄(CO)₁₂ (2.683(4) Å).^[23] The addition of a hydride ligand to **2-H** strongly distorts the Ir₃ cluster, as illustrated by the Ir...Ir distances within **5**: 2.7043(1), 2.9343(1), and 3.0164(1) Å.

Consistent with ¹H NMR data, crystallography reveals the location and coordination modes of seven hydride ligands: three terminal (H1, H2, H3), three bridging (H12, H13, H23), and one triply-bridging hydride (H123). The pyramidal coordination geometry of μ₃-H is characterized by an 89.8(2)° angle Ir–(μ₃-H)–Ir and 173.7(5)° angle P–Ir–(μ₃-H). As expected, average lengths of Ir–H bonds involving terminal H (1.580(2) Å) and μ₃-H (1.929(12) Å) are consistent with the proposed bond orders. Surprisingly, μ-H groups are asymmetrical, with short (1.684(4) Å) and long (1.945(4) Å) Ir–(μ-H) bonds that mimic the lengths of Ir–H and Ir–(μ₃-H), respectively, appropriate for a trans effect of the terminal hydrides. Despite the similar lengths of Ir–(μ₃-H) and long Ir–(μ-H) bonds, we see that only Ir–(μ₃-H) bond dissociates during the hydrogenation of **2-H** or carbonylation of [Ir₃H₇(dppp)₃]²⁺.^[15]

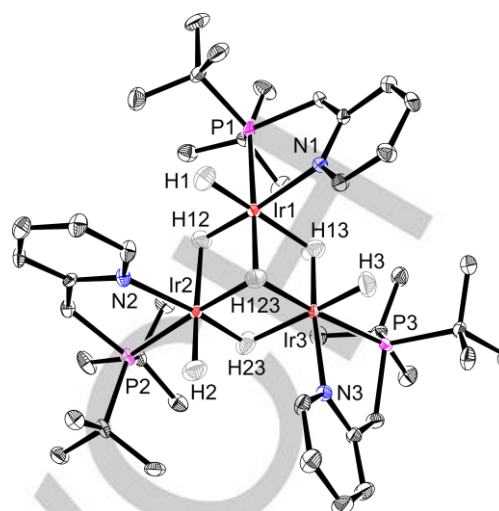


Figure 2. Molecular structure of the cation in [**2-H**](OTf)₂×CH₂Cl₂ showing localized hydride ligands (50% probability ellipsoids). Hydrogen atoms of the PN ligands are omitted for clarity.

Table 3. Selected interatomic distances (Å) in **2-H** determined by neutron crystallography. Values in parentheses indicate ±σ.

	Ir–H	Ir–(μ–H) short	Ir–(μ–H) long	Ir–(μ ₃ –H)	Ir...Ir
Ir1	1.577(7)	1.682(6)	1.947(7)	1.917(7)	Ir3 2.712(3)
Ir2	1.581(7)	1.690(7)	1.949(7)	1.945(7)	Ir1 2.734(3)
Ir3	1.581(6)	1.681(6)	1.939(7)	1.925(7)	Ir2 2.727(3)

NVS and FTIR Studies on 2-H. While crystallography has given some structural insight into which hydrides in the cluster might be involved in CO₂ reactivity, we sought dynamic information about the lability of these groups. Neutron vibrational spectroscopy (NVS) measurements were performed to interrogate iridium-hydride bonding in complex **2-H**. NVS probes the vibrational states of a crystalline sample without the selection rules applying to optical spectroscopies. NVS probes all vibrations across the Brillouin zone, and the modes involving displacement of H atoms are particularly intense due to the high total neutron scattering cross-sections of H atoms. Lastly, experimental NV spectra can be readily simulated using quantum chemistry computations, which greatly facilitates the NV mode assignment.

For this measurement, we synthesized the deuterated isotopologue [**2-H-d₇₂**](PF₆)₂ containing on average 80% D across all sites of the PN ligand, while maintaining 100% H in the Ir₃H₇ core. The large total scattering cross section of H atoms (82.03 barn) compared to D atoms (7.64 barn)^[24] allowed us to identify the phonon modes involving the Ir₃H₇ core in complex **2-H** with partially deuterated PN ligands. As expected, the experimental NV spectrum of **2-H-d₇₂** displays intense bands of the Ir₃H₇ cluster and much weaker bands of PN ligands (Figure 3, black curve). We conducted DFT calculations (see the supporting information) to simulate the NV spectrum of [**2-H-d₇₂**](PF₆)₂ (red curve), taking

RESEARCH ARTICLE

into account the deuterium content of each CH site and the spectrum of the isolated Ir_3H_7 cluster (blue curve), by setting the neutron scattering cross sections of selected atoms to zero. The NV bands observed in the simulated spectra agree very well with the experimental NV bands of $[\mathbf{2-H-d}_{72}](\text{PF}_6)_2$ and IR bands of $[\mathbf{2-H}](\text{PF}_6)_2$. The calculations also allow us to visualize^[25] the atomic displacements associated with the major phonon modes ν_1 – ν_6 of the Ir_3H_7 core (Table 4).

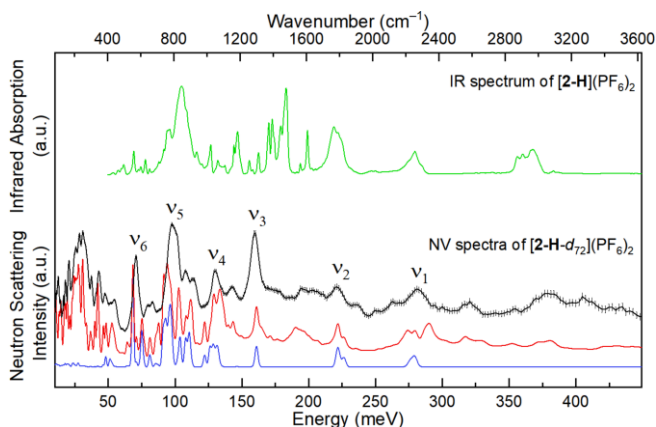


Figure 3. Comparison of the vibrational spectra: experimental IR of $[\mathbf{2-H}](\text{PF}_6)_2$ (green), experimental NV of $[\mathbf{2-H-d}_{72}](\text{PF}_6)_2$ (black, error bars = $\pm\sigma$), and simulated NV of $[\mathbf{2-H-d}_{72}](\text{PF}_6)_2$ (red) and Ir_3H_7 cluster with fundamental excitations only (blue).

The experimental NV spectrum shows two intense low energy bands at 573 cm^{-1} and 782 cm^{-1} (ν_6 and ν_5) that were assigned to bending modes: a rocking vibration of H1, H12, and H13 atoms in the plane orthogonal to $\text{P-Ir}(\mu_3\text{-H})$ axis and a scissoring vibration of the H1-Ir1-H12 fragment. A higher energy band ν_4 occurs at 1040 cm^{-1} and corresponds to a stretching vibration of the long $\text{Ir}(\mu\text{-H})$ bond *trans* to the terminal hydride. A strong band at 1290 cm^{-1} (ν_3) arises from a symmetrical stretching vibration of $\mu_3\text{-H}$ atom along the principal C_3 axis. A weak band at 1782 cm^{-1} (ν_2) was assigned to a stretching vibration of the short $\text{Ir}(\mu\text{-H})$ bond *trans* to the N atom. The distinct bond strengths of the long and short $\text{Ir}(\mu\text{-H})$ bonds are elegantly reflected by the 742 cm^{-1} difference in ν_2 and ν_4 , consistent with the bond length difference of 0.261 \AA . Finally, a weak band at 2266 cm^{-1} (ν_1) was assigned to the highest energy stretching vibration of the terminal Ir-H bond. It is worth noting that the observed frequencies ν_1 , ν_2 , and ν_4 (but not ν_3) show a linear relationship with the matching Ir-H bond lengths in $\mathbf{2-H}$: $\nu(\text{cm}^{-1}) = 7355 - 3259 \times d(\text{\AA})$, $R^2 = 0.985$.^[26] An even better correlation is observed ($R^2 = 0.999$) between an average stretching frequency per Ir-H bond (ν') and a sum of Ir-H distances (Σd) associated with a specific hydride: $\nu'(\text{cm}^{-1}) = 2969 - 437 \times \Sigma d(\text{\AA})$. Among the three, $\mu_3\text{-H}$ has the lowest value of $\nu' = \nu_3/3 = 430\text{ cm}^{-1}$. Alternatively, according to the calculations, stretching frequencies of the individual $\text{Ir}(\mu_3\text{-H})$ bonds occur at ($869\text{--}894$) cm^{-1} , which are less energetic vibrations than $\nu_1\text{--}\nu_4$. Thus, the data suggest the bond $\text{Ir}(\mu_3\text{-H})$ to be the most labile, supporting the proposed mechanism in Scheme 2.

Table 4. Assignment of the vibrational modes in Ir_3H_7 cluster

Band	Experimental (cm^{-1})		Calculated (cm^{-1})	
	IR of $\mathbf{2-H}$	IR of $\mathbf{2-H-d}_r$	NV of $\mathbf{2-H-d}_{r2}$	NV of $\mathbf{2-H-d}_{r2}$
ν_1	2257	1613	2266	2225–2257
ν_2	1770	1276	1782	1789–1826
ν_3			1290	1298
ν_4			1040	1051–1064
ν_5			782	732–750
ν_6			573	551–554

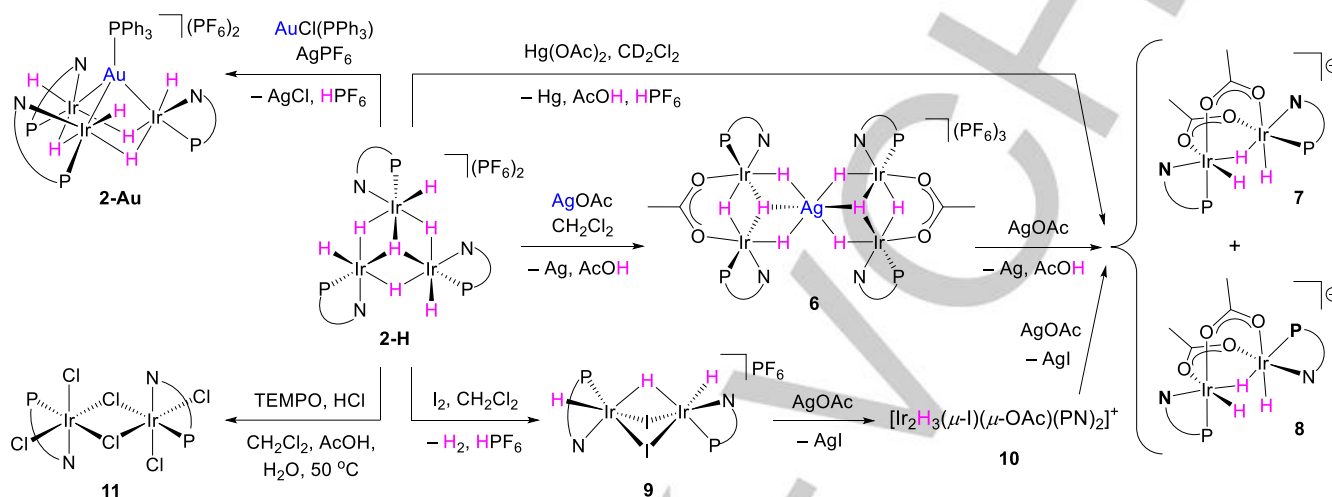
The NVS-DFT study enables the first thorough characterization of the vibrational modes of the Ir_3H_7 cluster. FTIR spectroscopy provides information on the high energy modes ν_1 and ν_2 , while the other relevant bands are obscured at lower energy. The IR spectrum of $[\mathbf{2-H}](\text{PF}_6)_2$ also contains ν_1 and ν_2 bands at 2257 cm^{-1} and 1770 cm^{-1} , respectively. These are shifted to lower frequencies at 1613 cm^{-1} and 1276 cm^{-1} when isotopologue $[\mathbf{2-H-d}_r](\text{PF}_6)_2$ featuring a deuterated Ir_3D_7 core was measured (Table 4). Typically, stretching bands of terminal Ir-H bonds in mononuclear complexes are strongly dependent on *trans* ligands and occur at ($2000\text{--}2300$) cm^{-1} .^[27–30] However, in complexes $[\text{Ir}_3\text{H}_7\text{L}_6]^{2+}$, the band ν_1 falls within a narrower range of ($2190\text{--}2240$) cm^{-1} due to the consistent presence of the *trans* $\mu\text{-H}$ ligand in all reported examples.^[12–16]

Oxidation of the Hydride Ligands in $\mathbf{2-H}$. We pursued stoichiometric reactivity studies on the Ir_3H_7 cluster to develop an intuition of its redox behavior. Complex $\mathbf{2-H}$ is inert to CH_3I , CH_3OTf , and $[\text{CPh}_3]\text{BF}_4$, suggesting low nucleophilicity of its hydride ligands. Furthermore, compound $[\mathbf{2-H}](\text{OTf})_2$ demonstrates very surprising stability in neat $\text{CF}_3\text{SO}_3\text{D}$ at $25\text{ }^\circ\text{C}$: ^1H NMR shows no decomposition or HD gas formation. However, the hydride ligands undergo H/D exchange at all three sites with different relative rates. After 3 days in neat $\text{CF}_3\text{SO}_3\text{D}$ at $25\text{ }^\circ\text{C}$, we noticed that the terminal hydrides exchange significantly faster (94% D, $\delta_{\text{H}} = -23.04\text{ ppm}$) than $\mu\text{-H}$ (49% D, $\delta_{\text{H}} = -18.56\text{ ppm}$) and $\mu_3\text{-H}$ (50% D, $\delta_{\text{H}} = -4.10\text{ ppm}$). No H/D exchange was detected in CD_3OD . We show that $\mu_3\text{-H}$ can be displaced selectively by Au(I) electrophiles. For example, treating $[\mathbf{2-H}](\text{PF}_6)_2$ with AuPPh_3^+ , generated *in situ* from $\text{AuCl}(\text{PPh}_3)$ and AgPF_6 , gives tetranuclear complex $[\text{Ir}_3\text{H}_6(\mu_3\text{-AuPPh}_3)(\text{PN})_3]^{2+}$ ($\mathbf{2-Au}$, Scheme 3). In contrast to $\mathbf{2-H}$ and $\mathbf{2-O}$, $\mathbf{2-Au}$ adopts nearly perfect tetrahedral geometry with Ir-Ir and Ir-Au distances ranging between 2.74 \AA and 2.81 \AA . The Au-P bond is tilted by 13° from the expected principal C_3 axis. ^{31}P NMR, however, shows that $\mathbf{2-Au}$ is perfectly symmetric in a CD_2Cl_2 solution. While the average distance Au-Ir found in $\mathbf{2-Au}$ ($2.779(24)\text{ \AA}$) is consistent with those in structures featuring $\text{R}_3\text{PAu}(\eta^3\text{-Ir}_3)$ and $\text{Ir}_3\text{H}_6(\mu_3\text{-AuX})$ cores: $[\text{Ph}_3\text{PAu}(\text{Ir}_6(\text{CO})_{15})]^-$ ($2.838(13)\text{ \AA}$),^[31]

RESEARCH ARTICLE

$[\text{Ph}_3\text{PAu}\{\text{Ir}_6\text{Ru}_3(\text{CO})_{21}\}]^-$ (2.831(18) Å),^[32] and $[\text{Ir}_3\text{H}_6(\mu_3\text{-AuNO}_3)(\text{dppe})_3]^+$ (2.705(10) Å),^[33] it is not clear whether Au and Ir are bound directly or via bridging hydrides. Strong spin coupling between the phosphorus nuclei of PN and PPh_3 ($^3J_{\text{PP}} = 41$ Hz) in the ^{31}P NMR spectrum favors three covalent bonds Au–Ir. This

description is also consistent with $^2J_{\text{PH}}$ coupling constants of the hydride ligands ($\delta_{\text{H}} = -20.61$ and -20.97 ppm) that were not affected by the installation of AuPPh_3 group.



Scheme 3. Oxidation of $[\mathbf{2-H}](\text{PF}_6)_2$. Complexes **2-Au**, **6**, **9**, and **11** were characterized by X-ray crystallography (Figure S71).

Complex **2-H** is stable to aerobic oxidation: $[\mathbf{2-H}](\text{PF}_6)_2$ withstands heating to 200 °C in air in a glass capillary. Redox potentials of $[\mathbf{2-H}](\text{PF}_6)_2$ were studied by cyclic voltammetry in a solution of $\text{CH}_2\text{Cl}_2/\text{CH}_3\text{OH}/\text{H}_2\text{O}$ (Figure S69). Upon scanning anodically, two chemically irreversible oxidation events were detected at 0.95 V and 1.96 V (vs. SHE at 200 mV/s). Oxidation at 0.95 V seems to cause the removal of $\mu_3\text{-H}$ ligand followed by dissociation of the trinuclear structure. We interrogated this pathway by controlled chemical oxidation using AgOAc , $\text{Hg}(\text{OAc})_2$, and I_2 (Scheme 3).

Compound $[\mathbf{2-H}](\text{PF}_6)_2$ slowly reacts with an excess of AgOAc ($E^\circ_{\text{Ag}^+/\text{Ag}} = 0.799$ V vs. SHE)^[34] in CH_2Cl_2 over days, forming a bright orange pentanuclear heterometallic complex $[\text{AgIr}_4\text{H}_8(\mu\text{-OAc})_2(\text{PN})_4]^{3+}$ (**6**), that was isolated in 50% yield. It features two identical fragments *syn*- $\text{Ir}_2\text{H}_4(\mu\text{-OAc})(\text{PN})_2^+$ coordinating Ag^+ in a centrosymmetric fashion. ^1H NMR data are consistent with eight hydrides, respectively, at -4.75 ppm (2H), -21.85 ppm (4H), and -30.78 ppm (2H). Average interatomic distances Ir–Ir and Ir–Ag are 2.653(1) Å and 2.885(38) Å, respectively, consistent with bonding between the metals via hydride bridges rather than Ag–Ir bonds: Ag–Ir distances in **6** are 0.176 Å longer than in the complex $[\text{Ag}\{(\mu\text{-H})_3\text{Ir}(\text{PPh}_3)_3\}_2]^+$ (2.709(1) Å), also containing AgH_6 polyhedron.^[35] The independent synthesis and characterization of complexes *anti*- $[\text{Ir}_2\text{H}_4(\mu\text{-O}_2\text{CR})(\text{PN})_2]^+$ has been documented.^[36] Formation of **6** is a window into how **2-H** opens. We envisage each metal of **2-H** bringing two hydrides to **6**, leaving one hydride, apparent $\mu_3\text{-H}$, cleaved oxidatively.

As the reaction with AgOAc continues, complex **6** is oxidized further to a mixture of diastereomeric cations **7** and **8** (1:12 ratio, Figure S65). Complex **7** was previously characterized as a *meso*

isomer of $[\text{Ir}_2\text{H}_3(\mu\text{-OAc})_2(\text{PN})_2]^+$,^[5] thus presaging a route by which **2-H** could be converted to a known formic acid dehydrogenation catalyst. Complex **8** is an asymmetric isomer of $[\text{Ir}_2\text{H}_3(\mu\text{-OAc})_2(\text{PN})_2]^+$ (*vide infra*).

In contrast to AgOAc , oxidation of $[\mathbf{2-H}](\text{PF}_6)_2$ with $\text{Hg}(\text{OAc})_2$ ($E^\circ_{\text{Hg}^{2+}/\text{Hg}} = 0.852$ V vs. SHE)^[34] in CD_2Cl_2 is fast and non-selective, as indicated by immediate precipitation of metallic mercury and generation of a complex mixture of products in the resulting solution (Figure S66). However, after three days, the initially formed intermediates converge to complexes **7** and **8** in a 1:1 ratio. We infer that this pathway is likely analogous to the one available for reactions of AgOAc .

Compound $[\mathbf{2-H}](\text{PF}_6)_2$ reacts quantitatively with 1.5 equivalents of I_2 ($E^\circ_{\text{I}_2/\text{I}^-} = 0.789$ V vs. SHE)^[34] in CH_2Cl_2 to give a bright yellow dinuclear complex $[\text{Ir}_2\text{H}_3(\mu\text{-I})_2(\text{PN})_2]^+$ (**9**). Similar to the $\text{Hg}(\text{OAc})_2$ reaction, the initial fast iodination produces a mixture of intermediates that equilibrate selectively to **9** within 5 hours (Figure S67). H_2 gas was detected as one of the reaction products ($\delta_{\text{H}} = 4.60$ ppm), which is expected, as further oxidation of H_2 to HI is endergonic ($\Delta G = +1.7$ kJ/mol). Compound $[\mathbf{9}]\text{PF}_6$ was isolated in 77% yield. The structure of **9** was confirmed by X-ray crystallography (Figure S71). Unfortunately, the poor quality of its crystals limits us to presenting this structure for connectivity only: we could not localize all anions in the unit cell. The cation contains two distinct $\text{Ir}(\text{PN})$ fragments that cause the bridging hydride ($\delta_{\text{H}} = -18.72$ ppm) to appear as a doublet of doublets with a larger coupling constant associated with *trans*-PH spin coupling ($^2J_{\text{PH}} = 48$ Hz). The same coupling pattern was observed for the bridging hydride in complex **8** ($\delta_{\text{H}} = -19.57$ ppm, $^2J_{\text{trans-PH}} = 51$ Hz), which supports the structure assignment. Further, treating $[\mathbf{9}]\text{PF}_6$

RESEARCH ARTICLE

with AgOAc in CD₂Cl₂ solution generates a mixture of acetato derivatives **7** and **8** (3:4 ratio, Figure S68) via an asymmetric mixed-ligand intermediate [Ir₂H₃(μ-I)(μ-OAc)(PN)₂]⁺ (**10**), which also features the characteristic signal of the bridging hydride ($\delta_{\text{H}} = -18.30$ ppm, $^2J_{\text{trans-PH}} = 50$ Hz).

The described experiments illustrate the high thermodynamic stability of class [Ir₂H₃(μ-X)₂(PN)₂]⁺ (X = I, OAc) with selective reactivity of μ₃-H ahead of other hydrides in the starting cluster. Still, the remaining hydrides can also be oxidized altogether. Under more forcing conditions, TEMPO and aqueous HCl oxidize [**2-H**](PF₆)₂ to red [Ir₂Cl₄(μ-Cl)₂(PN)₂] (**11**) within 17 hours at 50 °C (Scheme 3). The product is insoluble in common solvents, but X-ray diffraction-quality crystals were obtained by running the oxidation in the AcOH/CH₂Cl₂ solvent system. The distance between Ir atoms in complex **11** (3.715 Å) is ca. 1 Å longer than in its hydride-bridged congeners.

Overall, we see that under appropriate oxidative conditions, **2-H** can generate at least four classes of iridium complexes of varied nuclearity and hydride content: [Ir₃H₆X(PN)₃]²⁺ (X = AuPPh₃), Ir₂H₄X(PN)₂⁺ (X = OAc), [Ir₂H₃X₂(PN)₂]⁺ (X = I, OAc), and [Ir₂X₆(PN)₂] (X = Cl). Having screened a wide range of reagents, we noticed a correlation between the nature of an oxidant and the reaction kinetics. While elemental iodine, AuPPh₃⁺, and acetates of Ag(I) and Hg(II) work well at room temperature due to their ability to coordinate with the hydride ligands or enable direct electron transfer from Ir–H bonds; reagents that lack these properties (NBS, CBr₄, Me₃NO, TEMPO, PhI(OAc)₂, and PhHgOAc) show no reactivity or require forcing conditions (TEMPO/HCl system).

Conclusion

We conducted a comprehensive study on complex **2-H** that involved complete structural characterization and detailed analysis of the vibrational modes. We identified the stability limits of **2-H** to oxidation and identified the hydride source in its synthesis. Complex **2-H** demonstrated unexpected catalytic activity in reversible CO₂ hydrogenation enabled by the metal-metal cooperation within the triiridium cluster. The combined structural, vibrational, and reactivity data support a mechanism in which the Ir₃H₇ cluster initially opens by cleavage of its central μ₃-H and addition of an extra hydride. The hydride transfer from poorly nucleophilic cluster Ir₃H₈ to CO₂ requires elevated temperatures. The high stability of cluster Ir₃H₇ favors the recovery of **2-H** and thus enables a turnover (TON_{max} ≈ 30k).

Conflict of Interest

The authors declare no competing financial interest.

Acknowledgments

This work is sponsored by the U.S. Department of Energy, Office of Energy Efficiency and Renewable Energy (DE-EE-

00011096). NIST contributed to performing this work. We thank the NSF (CHE-2018740, DBI-0821671, CHE-0840366), the NIH (S10 RR25432), and USC Research and Innovation Instrumentation Awards for analytical equipment. Single-crystal neutron diffraction and vibrational spectroscopy measurements performed on TOPAZ and VISION beamlines used resources at the Spallation Neutron Source, a DOE Office of Science User Facility operated by the Oak Ridge National Laboratory (ORNL). Computing resources were made available through the VirtuES and the ICE-MAN projects, funded by Laboratory Directed Research and Development program and Compute and Data Environment for Science (CADES) at ORNL. We are grateful to Dr. William Richards (USC), Juan Pablo De Los Rios (USC), and Dr. Thomas Saal (USC) for help with analytical equipment, and Dr. John Gordon (Brookhaven) for insightful discussions. Fellowship assistance from the Arnold and Mabel Beckman Foundation (A.J.C.) and NSF REU award CHE-1757942 (J.K.) is gratefully acknowledged. R.A.K. appreciates support from the U.S. DOE Office of Energy Efficiency and Renewable Energy (EERE), Hydrogen and Fuel Cell Technologies Office (contract no. DE-AC36-8GO28308) to the National Renewable Energy Laboratory (NREL).

Certain commercial equipment, instruments, or materials are identified in this document. Such identification does not imply recommendation or endorsement by the National Institute of Standards and Technology, nor does it imply that the products identified are necessarily the best available for the purpose.

Keywords: catalysis • metal hydride • formate • heterometallic cluster • oxidation

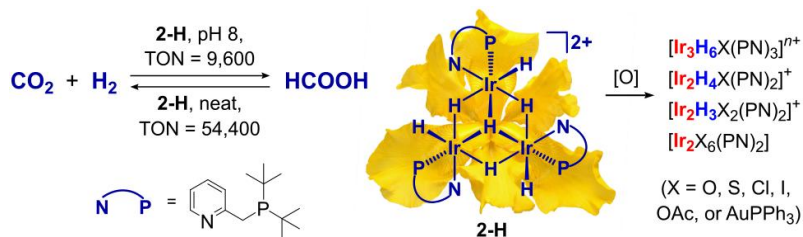
- [1] S. Kushwaha, J. Parthiban, S. K. Singh, *ACS Omega* **2023**, *8*, 38773.
- [2] Z. Ma, U. Legrand, E. Pahija, J. R. Tavares, D. C. Boffito, *Ind. Eng. Chem. Res.* **2021**, *60*, 803.
- [3] W.-H. Wang, J. F. Hull, J. T. Muckerman, E. Fujita, Y. Himeda, *Energy Environ. Sci.* **2012**, *5*, 7923.
- [4] S. Siangwata, A. Hamilton, G. J. Tizzard, S. J. Coles, G. R. Owen, *ChemCatChem* **2024**, *16*, e202301627.
- [5] J. J. A. Celaje, Z. Lu, E. A. Kedzie, N. J. Terrile, J. N. Lo, T. J. Williams, *Nature Commun.* **2016**, *7*, 11308.
- [6] R. Tanaka, M. Yamashita, K. Nozaki, *J. Am. Chem. Soc.* **2009**, *131*, 14168.
- [7] Y.-Q. Zhang, Y. Zhang, G. Zeng, R.-Z. Liao, M. Li, *Dalton Trans.* **2024**, 53, 684.
- [8] S. Semwal, A. Kumar, J. Choudhury, *Catal. Sci. Technol.* **2018**, *8*, 6137.
- [9] J. Guo, M. Li, C. Yin, D. Zhong, Y. Zhang, X. Li, Y. Wang, J. Yuan, H. Xie, T. Qi, *Inorg. Chem.* **2023**, *62*, 18982.
- [10] R. Kanega, M. Z. Ertem, N. Onishi, D. J. Szalda, E. Fujita, Y. Himeda, *Organometallics* **2020**, *39*, 1519.
- [11] Z. Wang, S.-M. Lu, J. Li, J. Wang, C. Li, *Chem. Eur. J.* **2015**, *21*, 12592.
- [12] D. F. Chodosh, R. H. Crabtree, H. Felkin, G. E. Morris, *J. Organomet. Chem.* **1978**, *161*, C67.
- [13] D. F. Chodosh, R. H. Crabtree, H. Felkin, S. Morehouse, G. E. Morris, *Inorg. Chem.* **1982**, *21*, 1307.
- [14] H. H. Wang, L. H. Pignolet, *Inorg. Chem.* **1980**, *19*, 1470.
- [15] H. H. Wang, A. L. Casalnuovo, B. J. Johnson, A. M. Mueting, L. H. Pignolet, *Inorg. Chem.* **1988**, *27*, 325.

RESEARCH ARTICLE

- [16] S. P. Smidt, A. Pfaltz, E. Martínez-Viviente, P. S. Pregosin, A. Albinati, *Organometallics* **2003**, *22*, 1000.
- [17] P. J. Lauridsen, Z. Lu, J. J. A. Celaje, E. A. Kedzie, T. J. Williams, *Dalton Trans.* **2018**, *47*, 13559.
- [18] N. Alfonso, V. K. Do, A. J. Chavez, Y. Chen, T. J. Williams, *Catal. Sci. Technol.* **2021**, *11*, 2361.
- [19] Z. Lu, V. Cherepakhin, I. Demianets, P. J. Lauridsen, T. J. Williams, *Chem. Commun.* **2018**, *54*, 7711.
- [20] V. K. Do, N. A. Vargas, A. J. Chavez, L. Zhang, V. Cherepakhin, Z. Lu, R. P. Currier, P. A. Dub, J. C. Gordon, T. J. Williams, *Catal. Sci. Technol.* **2022**, *12*, 7182.
- [21] S. Gruber, M. Neuburger, A. Pfaltz, *Organometallics* **2013**, *32*, 4702.
- [22] M.-A. Muller, S. Gruber, A. Pfaltz, *Adv. Synth. Catal.* **2018**, *360*, 1340.
- [23] M. R. Churchill, J. P. Hutchinson, *Inorg. Chem.* **1978**, *17*, 3528.
- [24] V. F. Sears, *Neutron News* **1992**, *3*, 26.
- [25] The animations are supplied as an SI file (.phonon), which can be viewed via the software package Jmol. <http://www.jmol.org/>
- [26] J. A. Larsson, D. Cremer, *J. Mol. Struct.* **1999**, *485-486*, 385.
- [27] R. H. Morris, *Inorg. Chem.* **2018**, *57*, 13809.
- [28] M. A. Esteruelas, M. Oliván, A. Vélez, *Inorg. Chem.* **2013**, *52*, 12108.
- [29] J. C. Lee, A. L. Rheingold, B. Muller, P. S. Pregosin, R. H. Crabtree, *J. Chem. Soc., Chem. Commun.* **1994**, 1021.
- [30] S. A. Smith, D. M. Blake, M. Kubota, *Inorg. Chem.* **1972**, *11*, 660.
- [31] R. D. Pergola, F. Demartin, L. Garlaschelli, M. Manassero, S. Martinengo, N. Masciocchi, M. Sansoni, *Organometallics* **1991**, *10*, 2239.
- [32] T. Chihara, M. Sato, H. Konomoto, S. Kamiguchi, H. Ogawa, Y. Wakatsuki, *J. Chem. Soc., Dalton Trans.* **2000**, 2295.
- [33] A. L. Casalnuovo, L. H. Pignolet, J. W. A. van der Velden, J. J. Bour, J. J. Steggerda, *J. Am. Chem. Soc.* **1983**, *105*, 5957.
- [34] S. G. Bratsch, *J. Phys. Chem. Ref. Data* **1989**, *18*, 1.
- [35] F. Bachechi, *J. Organomet. Chem.* **1994**, *474*, 191.
- [36] M.-L. Li, S. Yang, X.-C. Su, H.-L. Wu, L.-L. Yang, S.-F. Zhu, Q.-L. Zhou, *J. Am. Chem. Soc.* **2017**, *139*, 541.
- [37] Deposition numbers 2289546, 2235972 (for $[2\text{-H}](\text{OTf})_2 \times \text{CH}_2\text{Cl}_2$), 2289544 (for $[2\text{-O}]\text{OTf}$), 2289547 (for $[2\text{-Au}](\text{BF}_4)(\text{PF}_6)$), 2382865 (for $[5]\text{PF}_6 \times 2\text{CH}_2\text{Cl}_2$), 2289545 (for $[6](\text{PF}_6)_3 \times \frac{1}{4}\text{CH}_2\text{Cl}_2$), and 2289543 (for $10 \times \text{CH}_2\text{Cl}_2$) contain the supplementary crystallographic data for this paper. These data are provided free of charge by the joint Cambridge Crystallographic Data Centre and Fachinformationszentrum Karlsruhe [Access Structures](#) service.

RESEARCH ARTICLE

Entry for the Table of Contents



A novel triiridium heptahydride cluster catalyzes reversible CO₂ hydrogenation. Foundational structural and reactivity studies that combine neutron crystallography and spectroscopy, electrochemistry, synthetic studies, and kinetics uncover previously elusive metal-metal cooperative reactivity that enables a unique approach to functionalize CO₂.